

TIDAL STIRRING OF DISKY DWARFS WITH SHALLOW DARK MATTER DENSITY PROFILES: ENHANCED TRANSFORMATION INTO DWARF SPHEROIDALS

STELIOS KAZANTZIDIS¹, EWA L. LOKAS², AND LUCIO MAYER³

Accepted by ApJL on January 26, 2013

ABSTRACT

The origin of dwarf spheroidal galaxies (dSphs) in the Local Group (LG) remains an enigma. The tidal stirring model posits that late-type, rotationally-supported dwarfs resembling present-day dwarf irregular (dIrr) galaxies can transform into dSphs via interactions with Milky Way-sized hosts. Using collisionless N -body simulations, we investigate for the first time how tidal stirring depends on the dark matter (DM) density distribution in the central stellar region of the progenitor disk dwarf. Specifically, we explore various asymptotic inner slopes γ of the dwarf DM density profiles ($\rho \propto r^{-\gamma}$ as $r \rightarrow 0$). For a given orbit inside the primary galaxy, rotationally-supported dwarfs embedded in DM halos with core-like density distributions ($\gamma = 0.2$) and mild density cusps ($\gamma = 0.6$) demonstrate a substantially enhanced likelihood and efficiency of transformation into dSphs compared to their counterparts with steeper DM density profiles ($\gamma = 1$). Such shallow DM distributions are akin to those of observed dIrrs, highlighting tidal stirring as a plausible model for the origin of the morphology-density relation in the LG. When $\gamma < 1$, a single pericentric passage can induce dSph formation and disk dwarfs on low-eccentricity or large-pericenter orbits are able to transform into dSphs; these new results allow the tidal stirring model to explain the existence of virtually all known dSphs across a wide range of distances from their hosts. A subset of rotationally-supported dwarfs initially embedded in DM halos with shallow density profiles are eventually disrupted by the primary galaxy; those that survive as dSphs are generally on orbits that are biased towards lower eccentricities and/or larger pericenters relative to those of typical cold dark matter (CDM) satellites. The latter could explain the rather peculiar orbits of several classic LG dSphs such as Fornax, Leo I, Tucana, and Cetus. We conclude that tidal stirring constitutes a prevalent evolutionary mechanism for shaping the nature of dwarf galaxies within the currently favored CDM cosmological paradigm.

Subject headings: galaxies: dwarf – galaxies: Local Group – galaxies: kinematics and dynamics – galaxies: formation – methods: numerical

1. INTRODUCTION

The dwarf spheroidal (dSph) satellites in the Local Group (LG) are the faintest and most dark-matter (DM) dominated galaxies known (e.g., Mateo 1998; Tolstoy et al. 2009). These intriguing objects exhibit no appreciable gas components and tend to be clustered around the massive spiral galaxies Milky Way (MW) and M31. Furthermore, dSphs are characterized by pressure-supported, spheroidal stellar components (e.g., Mateo 1998) and a wide diversity of star formation histories (e.g., Orban et al. 2008). Despite recent advances in our understanding of dSphs, a conclusive model for their origin has yet to emerge (e.g., Kravtsov 2010).

One class of models attempts to explain the formation of dSphs via environmental processes, including tidal and ram pressure stripping (e.g., Einasto et al. 1974; Faber & Lin 1983; Mayer et al. 2001; Kravtsov et al. 2004; Mayer et al. 2006, 2007; Klimentowski et al. 2009; Kazantzidis et al. 2011a; Lokas et al. 2011), mergers between dwarf galaxies (Kazantzidis et al. 2011b; Yozin & Bekki 2012), and resonant stripping

(D’Onghia et al. 2009). In this context, the “tidal stirring” model of Mayer et al. (2001) postulates that interactions with MW-sized host galaxies can transform late-type, rotationally-supported dwarfs resembling present-day dwarf irregular (dIrr) galaxies into pressure-supported, spheroidal stellar systems with the kinematic and structural properties of the *classic* LG dSphs (see Lokas et al. 2012a for an extension of this model to the newly-discovered ultra-faint dSphs).

Previous work on tidal stirring has almost exclusively adopted cuspy, Navarro et al. (1996, hereafter NFW) density profiles to model the DM halos of the progenitor disk dwarfs. Yet, rotation-curve modeling of observed dIrrs (e.g., Wdrazke et al. 2003; Oh et al. 2011), which constitute the most plausible predecessors of dSphs according to the tidal stirring model, favors DM halos with significantly shallower inner density slopes. Such shallow DM density distributions are also supported by hydrodynamical cosmological simulations of dwarf galaxy formation (Governato et al. 2010) and recent analytic models for the origin of core-like DM density profiles in dwarfs (Pontzen & Governato 2012).

Given that tidal stirring involves a combination of tidally-induced dynamical instabilities (e.g., bars) and impulsive tidal heating of the stellar component, the cuspieness of the dwarf DM density distribution in the central region where the stars reside should play a crucial role in this complex transformation mechanism. In-

¹ Center for Cosmology and Astro-Particle Physics; and Department of Physics; and Department of Astronomy, The Ohio State University, Columbus, OH 43210, USA; stelios@mps.ohio-state.edu

² Nicolaus Copernicus Astronomical Center, 00-716 Warsaw, Poland

³ Institute for Theoretical Physics, University of Zürich, CH-8057 Zürich, Switzerland

deed, disk dwarf galaxies with shallow DM density profiles are characterized by lower central densities and, correspondingly, longer internal dynamical times compared to their counterparts with steeper DM density distributions. Systems with longer dynamical times respond more impulsively to external tidal perturbations and suffer stronger tidal heating (e.g., Gnedin & Ostriker 1999). Rotationally-supported dwarf galaxies with progressively shallower DM density profiles may thus experience increasingly probable and efficient transformations into dSphs. Nonetheless, there has been no *quantitative* work aimed at investigating this qualitative expectation.

Here we explore this issue via a series of tidal stirring simulations of disk dwarfs embedded in DM halos with different inner density distributions. Our results demonstrate that the likelihood and efficiency of transformation into a dSph are both enhanced substantially when the progenitor rotationally-supported dwarfs possess shallow DM density profiles, whose slopes in the central stellar regions are in agreement with those inferred from recent theoretical and observational efforts in dwarf galaxy formation. These findings further establish tidal stirring as a prevalent evolutionary mechanism for shaping the nature of dwarf galaxies within the currently favored cold dark matter (CDM) cosmological paradigm.

2. METHODS

A description of the adopted methodology is given in Lokas et al. (2012a). For completeness, we provide a summary of our approach here. We employed the technique of Widrow et al. (2008) to construct numerical realizations of dwarf galaxies consisting of exponential stellar disks embedded in DM halos. The DM halo density profiles followed the general form (Lokas 2002),

$$\rho(r) = \frac{\rho_s}{(r/r_s)^\gamma (1 + r/r_s)^{3-\gamma}}, \quad (1)$$

where ρ_s , r_s , and γ denote the characteristic inner density, the scale radius, and the *asymptotic* inner slope of the profile, respectively. ρ_s depends on the epoch of halo formation, the present-day values of the cosmological parameters, and γ (throughout the paper we assume the concordance Λ CDM cosmogony and $z = 0$).

To examine how the DM density distribution in the central stellar region of the progenitor disk dwarf affects tidal stirring, we varied γ in three otherwise identically initialized dwarf galaxies. Specifically, we adopted $\gamma = 1$ (corresponding to the NFW profile) and two shallower inner slopes, namely a mild density cusp ($\gamma = 0.6$) and a nearly constant density core ($\gamma = 0.2$). These shallow power-law indices are well-motivated as they are akin to those of both observed dIrrs (e.g., Weldrake et al. 2003; Oh et al. 2011) and realistic dIrr-like systems formed in hydrodynamical cosmological simulations (Governato et al. 2010).

Each dwarf galaxy comprised a DM halo with a virial mass of $M_{\text{vir}} = 10^9 M_\odot$ (corresponding to a virial radius of $r_{\text{vir}} \approx 25.9$ kpc) and a concentration parameter of $c \equiv r_{\text{vir}}/r_s = 20$ ($r_s \approx 1.29$ kpc), and was exponentially truncated beyond r_{vir} (Kazantzidis et al. 2004a). All DM halos hosted an identical stellar disk whose mass, radial scale-length, sech^2 vertical scale-height, and central radial velocity dispersion were equal to $M_d = 0.02 M_{\text{vir}}$,

TABLE 1
ORBITAL PARAMETERS OF DISKY DWARFS

Orbit (1)	r_{apo} (kpc) (2)	$r_{\text{apo}}/r_{\text{peri}}$ (3)	r_{peri} (kpc) (4)	T_{orb} (Gyr) (5)
O1	125	5	25	2.1
O2	85	5	17	1.3
O3	250	5	50	5.4
O4	125	10	12.5	1.8
O5	125	2.5	50	2.5

$R_d \approx 0.41$ kpc, $z_d = 0.2 R_d$, and $\sigma_{R0} = 10 \text{ km s}^{-1}$, respectively (see Kazantzidis et al. 2011a for the motivation behind these parameter values). We note that the value of R_d is derived assuming a dimensionless halo spin parameter of $\lambda = 0.04$ (Mo et al. 1998). Being embedded in different DM density distributions, the resulting disks differed in their velocity dispersion profile and Toomre Q stability parameter (at $R = 2.5 R_d$, $Q \approx 3.8, 3.3$, and 2.9 for $\gamma = 1, 0.6$ and 0.2 , respectively; direct numerical simulations of the evolution of all dwarf galaxies in isolation for a period of 10 Gyr confirmed their stability against bar formation).

Our choices of γ above lead to DM density profiles, circular velocity profiles, and stellar binding energy distributions that display markedly dissimilar shapes within $5 R_d \approx 2$ kpc, namely the radius containing the vast majority ($\gtrsim 95\%$) of disk stars (see Figure 1 of Lokas et al. 2012a). Hence, although our modeling approach is certainly not unique, it does satisfy the main requirement of the present study by ensuring that the employed rotationally-supported dwarfs exhibit substantially different initial properties in the central stellar region. In particular, decreasing cusp slopes correspond to less concentrated mass and energy distributions, less steeply rising circular velocity profiles, and smaller maximum circular velocities V_{max} ($V_{\text{max}} \approx 19.6, 17.8$, and 16.7 km s^{-1} for $\gamma = 1, 0.6$ and 0.2 , respectively). Therefore, rotationally-supported dwarfs embedded in DM halos with shallow density profiles are expected to manifest rather different responses to tidal shocks and overall tidal evolutions compared to their counterparts with steeper DM density distributions. We shall quantify these differences in the following section.

The dwarf galaxy models contained $N_h = 10^6$ DM and $N_d = 5 \times 10^5$ disk particles with a gravitational softening of $\epsilon_h = 60$ pc and $\epsilon_d = 20$ pc, respectively. Resolution was adequate to resolve all scales of interest. We assumed a single host represented by a self-gravitating, high-resolution numerical model of the MW (Kazantzidis et al. 2011a). Each disk dwarf was placed on five bound orbits of varying sizes and eccentricities inside the primary galaxy, for a total of 15 experiments. In detail, we employed a subset of orbits from Kazantzidis et al. (2011a), whose parameters were motivated by both theoretical studies of the orbital distributions of cosmological halos in MW-sized hosts (e.g., Diemand et al. 2007; Klimentowski et al. 2010) and observational work pertaining to LG dwarfs (e.g., McConnachie 2012). Table 1 summarizes the adopted orbital parameters, including apocentric distances, r_{apo} ,

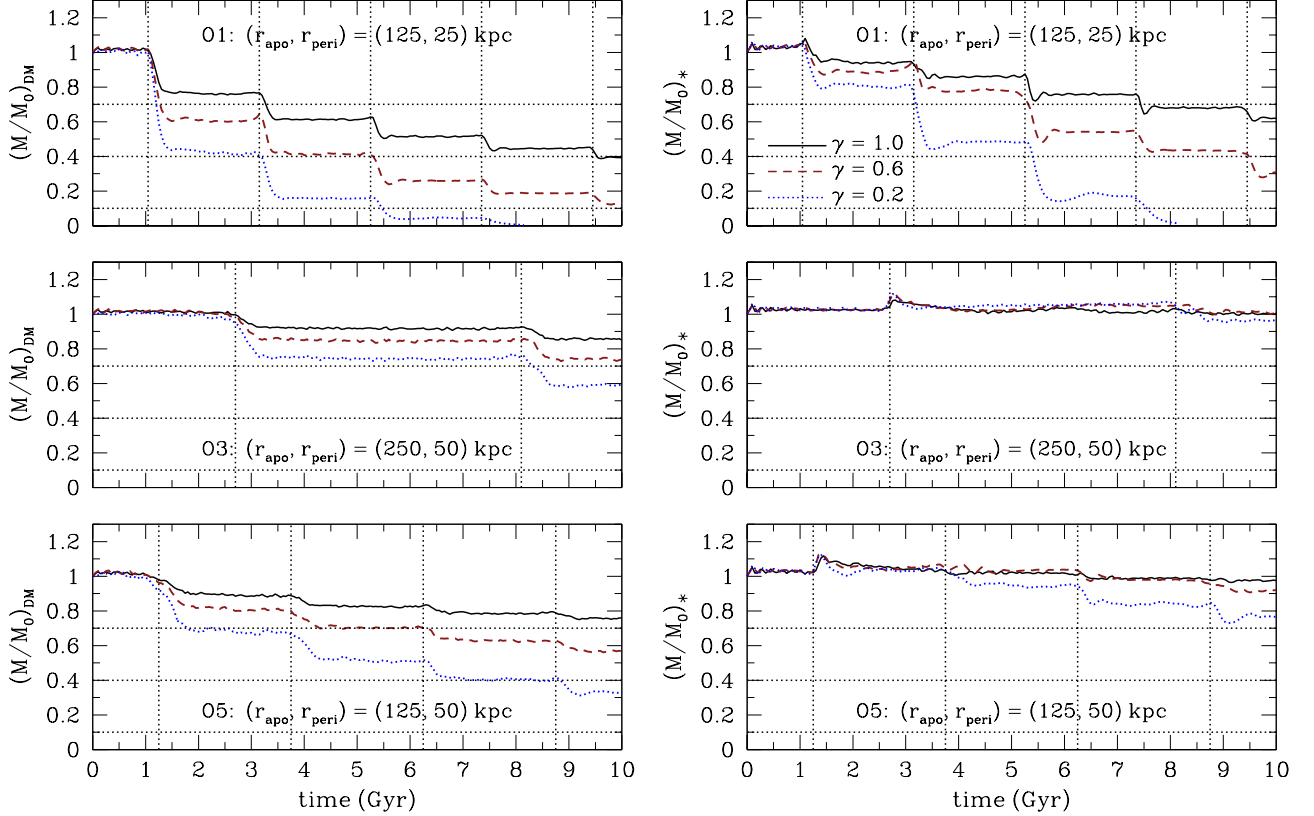


FIG. 1.— Evolution of mass in the DM (left panels) and stellar (right panels) components of the simulated disk dwarf galaxies as a function of time. Results are presented for orbits O1 (upper panels), O3 (middle panels), and O5 (lower panels). γ denotes the *asymptotic* inner slope of the dwarf DM density distribution and the solid, dashed, and dotted lines correspond to $\gamma = 1.0$, $\gamma = 0.6$, and $\gamma = 0.2$, respectively. DM (stellar) masses are computed within 0.7 kpc from the center of the dwarf (see text for details) and are normalized to the *initial* DM (stellar) mass enclosed within 0.7 kpc, M_0 . In all panels, vertical lines specify pericentric passages and horizontal lines indicate mass loss of 30%, 60%, and 90% with respect to the initial value. For a given orbit inside the host galaxy, rotationally-supported dwarfs embedded in DM halos with shallow density profiles ($\gamma < 1$) suffer enhanced mass loss compared to their counterparts with steeper DM density distributions ($\gamma = 1$).

eccentricities, $r_{\text{apo}}/r_{\text{peri}}$, pericentric distances, r_{peri} , and orbital times, T_{orb} . The dwarf galaxies, having considerably lower masses with respect to the host, do not experience dynamical friction (e.g., Colpi et al. 1999) and, as a result, their orbital parameters remain virtually unchanged during the course of their evolution. In all cases, the dwarfs started at apocenter and were evolved for 10 Gyr inside the primary. The alignments between the internal angular momenta of the dwarfs, those of the primary disks and the orbital angular momenta were all always prograde and equal to 45° (see Kazantzidis et al. 2011a regarding the implications of these choices). Lastly, the simulations were performed with the N -body code PKDGRAV (Stadel 2001).

3. RESULTS

We examined the global response of the disk dwarf galaxies subject to the tidal field of the host galaxy via the time evolution of their masses, kinematics, and shapes. These properties were always computed within 0.7 kpc from the dwarf center, a radius which is approximately equal to the half-light radius, $r_{1/2}$, of the initial disk. Adopting this well-defined, fixed scale facilitates meaningful comparisons among different experiments and enables us to overcome the complications associated with determining tidal radii (e.g., Read et al. 2006).

The dwarf kinematics and shapes were quantified

through the parameters V_{rot}/σ_* and c/a , where V_{rot} , σ_* , c , and a denote the rotational velocity, the one-dimensional velocity dispersion, the minor axis, and the major axis of the stellar distribution, respectively. At each simulation output, the following procedure was repeated. First, we determine the directions of the principal axes and derive c/a using the moments of the inertia tensor. Subsequently, we introduce a spherical coordinate system (r, θ, ϕ) , where ϕ is the angle coordinate in the xy plane oriented in such a way that the z -axis is along the minor axis of the stellar distribution. Lastly, we calculate V_{rot} around the minor axis $V_{\text{rot}} = V_\phi$ and compute the dispersions σ_r , σ_θ , and σ_ϕ around the mean values; σ_* , which we adopt throughout the paper as a measure of the amount of random motions in the stars, is defined as $\sigma_* \equiv [(\sigma_r^2 + \sigma_\theta^2 + \sigma_\phi^2)/3]^{1/2}$.

Given the typical parameters associated with orbit O1, we use it as the basis for the comparison with the other experiments. In what follows, we only describe results pertaining to orbits O1, O3, and O5. This is for brevity and because the evolution of the rotationally-supported dwarfs on the tightest (O2) and the most eccentric (O4) of our orbits displays similar salient features to those of O1. We emphasize that orbits O3 and O5 are characterized by larger pericenters and/or lower eccentricities compared to those of representative CDM satellites (e.g.,

TABLE 2
SUMMARY OF RESULTS

Simulation (1)	γ (2)	Orbit (3)	Survival (4)	t_d (Gyr) (5)	Bar Formation (6)	V_{rot}/σ_* (7)	c/a (8)	Classification (9)	t_{dSph} (Gyr) (10)
S1	1.0	O1	yes	—	yes	0.63	0.66	dSph?	—
S2	1.0	O2	yes	—	yes	0.01	0.93	dSph	2.85 (2)
S3	1.0	O3	yes	—	no	1.21	0.33	non-dSph	—
S4	1.0	O4	yes	—	yes	0.06	0.93	dSph	3.75 (2)
S5	1.0	O5	yes	—	no	1.11	0.38	non-dSph	—
S6	0.6	O1	yes	—	yes	0.01	0.82	dSph	5.55 (3)
S7	0.6	O2	no	6.40	yes	0.01	0.82	dSph	2.55 (2)
S8	0.6	O3	yes	—	no	0.92	0.40	non-dSph	—
S9	0.6	O4	no	9.30	yes	0.07	0.76	dSph	3.35 (2)
S10	0.6	O5	yes	—	yes	0.67	0.49	dSph?	—
S11	0.2	O1	no	8.15	yes	0.06	0.83	dSph	3.70 (2)
S12	0.2	O2	no	3.80	yes	0.07	0.82	dSph	1.85 (1)
S13	0.2	O3	yes	—	yes	0.63	0.47	dSph?	—
S14	0.2	O4	no	3.35	yes	0.15	0.68	dSph	2.60 (1)
S15	0.2	O5	yes	—	yes	0.64	0.56	dSph?	—

Diemand et al. 2007).

Figure 1 shows the time evolution of both DM and stellar mass of the simulated disk dwarf galaxies as they orbit inside the primary. Apart from illustrating the continuous stripping of the dwarf mass by the host tidal field, this figure highlights a number of additional generic features. First, masses decrease significantly at pericentric passages, where the intensity and variation of the time-dependent tidal forces are the strongest, and the tidal shocks occur. Between pericenters, masses remain remarkably constant, indicating that the dwarfs respond nearly adiabatically to the tidal field. Furthermore, the mass loss of the DM component greatly exceeds that of the stellar distribution, reflecting the more efficient tidal stripping of the *extended* DM halos of the dwarfs.

Second, irrespective of orbit, disk dwarf galaxies embedded in DM halos with shallow density profiles ($\gamma < 1$) suffer augmented mass loss in both stellar and DM components compared to their counterparts with steeper DM density distributions ($\gamma = 1$) (see Kazantzidis et al. 2004b; Peñarrubia et al. 2010 for similar conclusions; these studies, however, performed simulations of the tidal evolution of dwarfs without stellar disks). In some circumstances, the amount of mass loss is so dramatic that it leads to complete tidal disruption. Columns 4 and 5 of Table 2 provide information regarding dwarf survival (as indicated by the presence of a self-bound entity at $t = 10$ Gyr) and list the time of disruption if it occurs, respectively.

In Figure 2, we present the time evolution of the kinematics and shapes of the simulated disk dwarfs as they orbit inside the host galaxy. Given that V_{rot} is larger for more concentrated mass distributions and that all dwarf models are initialized with the same value of σ_{R0} , steeper cusp slopes result in greater initial values of V_{rot}/σ_* . We also note that the $\gamma = 0.2$ dwarf exhibits $V_{\text{rot}}/\sigma_* \approx 1$ initially. This notably low value of V_{rot}/σ_* for a disk is simply a consequence of our specific choice to compute the dwarf properties within 0.7 kpc from the center and

does not interfere with the interpretation of the results.

Injection of energy via tidal shocks at pericentric passages increases the random motions of disk stars, causing their orbits to become more isotropic. Thus, V_{rot}/σ_* progressively decreases, signifying the transition from rotationally-supported to pressure-supported stellar systems dominated by random motions. Simultaneously, the initially disk-like stellar distributions evolve into more spheroidal shapes as reflected in the continuous increase of c/a . Figure 2 shows that, regardless of orbit inside the primary, rotationally-supported dwarfs embedded in DM halos with shallow density profiles ($\gamma < 1$) demonstrate stronger evolution in their kinematics and shapes compared to their counterparts with steeper DM density distributions ($\gamma = 1$).

It is important to stress that the strong tidal forces at pericenters typically trigger bar instabilities in the disks of the dwarfs. These tidally-induced bars play a vital role in the overall decrease of V_{rot} by transporting angular momentum outwards. As tidal stripping removes the outer parts of the dwarfs, the entire angular momentum content progressively decreases and the ability of the dwarf galaxies to be supported by rotation progressively diminishes. The seemingly unexpected increase of V_{rot}/σ_* observed in Figure 2 between some pericentric passages is due to the particular orientation of these bars at the moment of pericenter crossing and the strong tidal torques exerted on them by the primary galaxy, resulting in an increase of V_{rot} (see Kazantzidis et al. 2011a). Column 6 of Table 2 indicates that bar formation is more probable in shallow DM density distributions (see also Mayer & Wadsley 2004).

Our primary goal is to assess the likelihood and efficiency of transformation into a dSph via tidal stirring. In accordance with observational studies of LG dwarf galaxies (e.g., Mateo 1998; McConnachie 2012), we classify as *bona fide* dSphs only those simulated systems whose final states are characterized by $V_{\text{rot}}/\sigma_* \lesssim 0.5$ and $c/a \gtrsim 0.5$. We underline that our theoretically derived values of

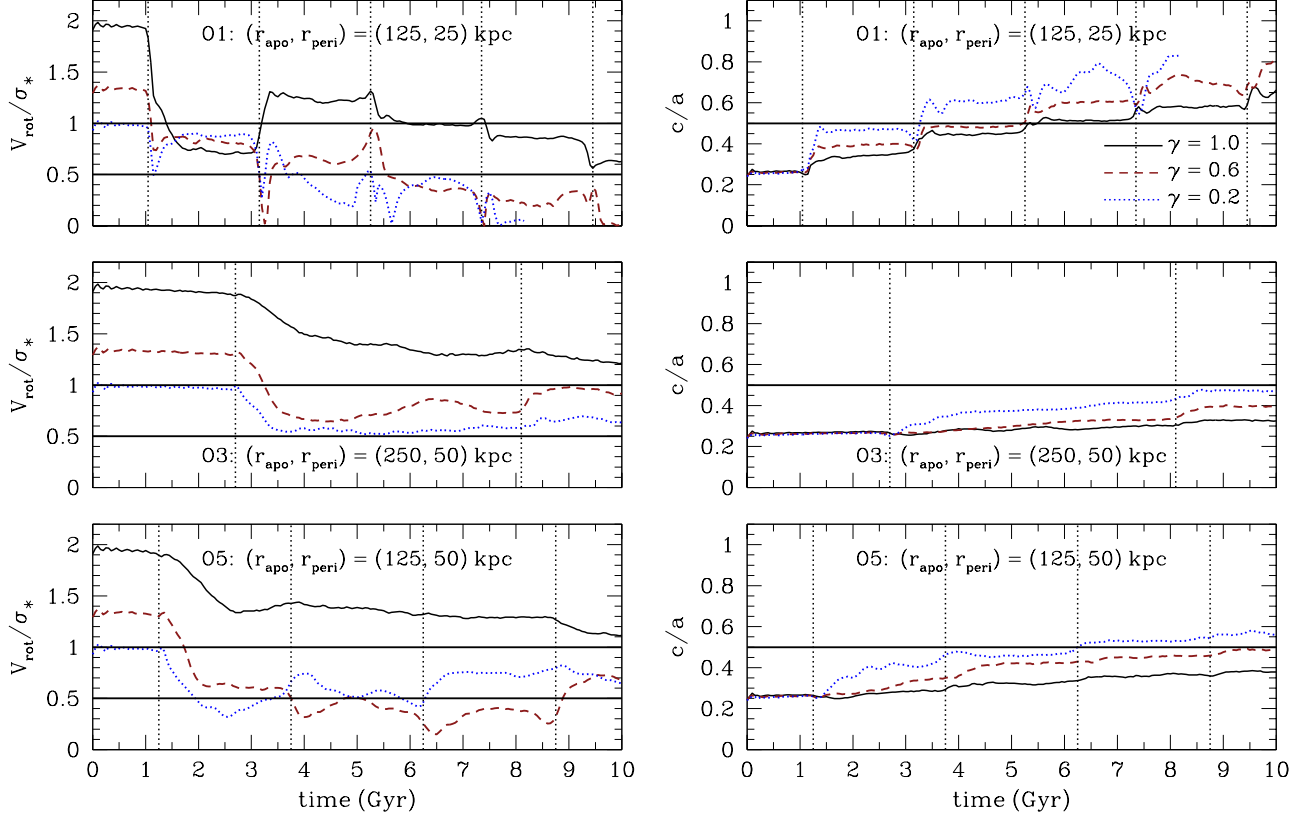


FIG. 2.— Evolution of stellar kinematics (left panels) and shape (right panels) of the simulated disk dwarf galaxies as a function of time. Results are presented for orbits O1 (upper panels), O3 (middle panels), and O5 (lower panels). Line types are as in Figure 1. V_{rot}/σ_* and c/a are computed within 0.7 kpc from the center of the dwarf (see text for details). Horizontal lines indicate the limiting values $V_{\text{rot}}/\sigma_* = 1$, $V_{\text{rot}}/\sigma_* = 0.5$, and $c/a = 0.5$: simulated dwarfs whose final states are characterized by $V_{\text{rot}}/\sigma_* \lesssim 0.5$ and $c/a \gtrsim 0.5$ correspond to *bona fide* dSphs, while those with final values of $0.5 \lesssim V_{\text{rot}}/\sigma_* \lesssim 1$ and $c/a \gtrsim 0.5$ are classified as “dSph?” (see text). For a given orbit inside the host, rotationally-supported dwarf galaxies embedded in DM halos with shallow density profiles ($\gamma < 1$) experience a stronger evolution in their shapes and kinematics and demonstrate a considerably enhanced likelihood and efficiency of transformation into dSph-like systems relative to their counterparts with steeper DM density distributions ($\gamma = 1$).

V_{rot}/σ_* and c/a are appropriate for meaningful comparisons with those of observed dSphs (see Kazantzidis et al. 2011a for a thorough discussion on this issue). In fact, the criterion $V_{\text{rot}}/\sigma_* \lesssim 0.5$ for establishing dSph formation in our experiments should be regarded as fairly conservative. Indeed, we measure V_{rot} around the minor axis of the stellar distribution, which corresponds to observing the simulated dwarfs perfectly edge-on. Consequently, V_{rot} is *nearly* equivalent to the maximum rotational velocity and, thus, the values of V_{rot}/σ_* that we quote throughout the paper are essentially the largest possible. Adopting a random line-of-sight would result in smaller V_{rot}/σ_* values, indicating even stronger and more complete transformations.

Columns 7 and 8 of Table 2 list the final values of V_{rot}/σ_* and c/a , respectively. These values correspond to different timescales (from ~ 4 to 10 Gyr) that are determined by the presence of a well-defined, bound stellar component of ~ 0.7 kpc in size. Column 9 reports whether a dSph was produced according to the two criteria above. The notation “dSph?” in this column is introduced to account for observed dSphs that exhibit $0.5 \lesssim V_{\text{rot}}/\sigma_* \lesssim 1$ such as Cetus (Lewis et al. 2007), Tucana (Fraternali et al. 2009), and Andromeda II (Ho et al. 2012). Of the disk dwarf galaxies initially embedded in cuspy DM halos ($\gamma = 1$), only those on high-eccentricity ($r_{\text{apo}}/r_{\text{peri}} \gtrsim 5$) and small-pericenter

($r_{\text{peri}} \lesssim 25$ kpc) orbits are transformed into objects with the properties of dSphs (see also Mayer et al. 2001; Kazantzidis et al. 2011a). Most importantly, the likelihood of dSph formation is enhanced significantly for shallow DM density profiles ($\gamma < 1$); in such cases, rotationally-supported dwarfs on previously unfavorable low-eccentricity and/or large-pericenter orbits are able to transform into dSph-like systems. Figure 3 shows the surface density maps of the final stellar components of the dwarfs and visually confirms these conclusions.

It is also worth emphasizing that, when $\gamma < 1$, a dSph can be created without significant mass loss in the stellar component (see Figure 1) because strong tidal shocks are not required to induce transformation for $\gamma = 0.6$ and $\gamma = 0.2$. This finding has interesting implications as it suggests that the presence or absence of prominent tidal tails in present-day dSphs may not constitute a robust observational constraint on the tidal stirring model without prior knowledge of the inner DM density distributions of such objects (Mayer et al. 2002).

Inspection of Columns 6 and 9 of Table 2 illustrates that dSph formation only occurs in conjunction with the development of bar instabilities, highlighting a strong association between bar formation and transformation into a dSph via tidal stirring (see also, e.g., Mayer et al. 2001; Klimentowski et al. 2009; Kazantzidis et al. 2011a). Lastly, Column 10 of Table 2

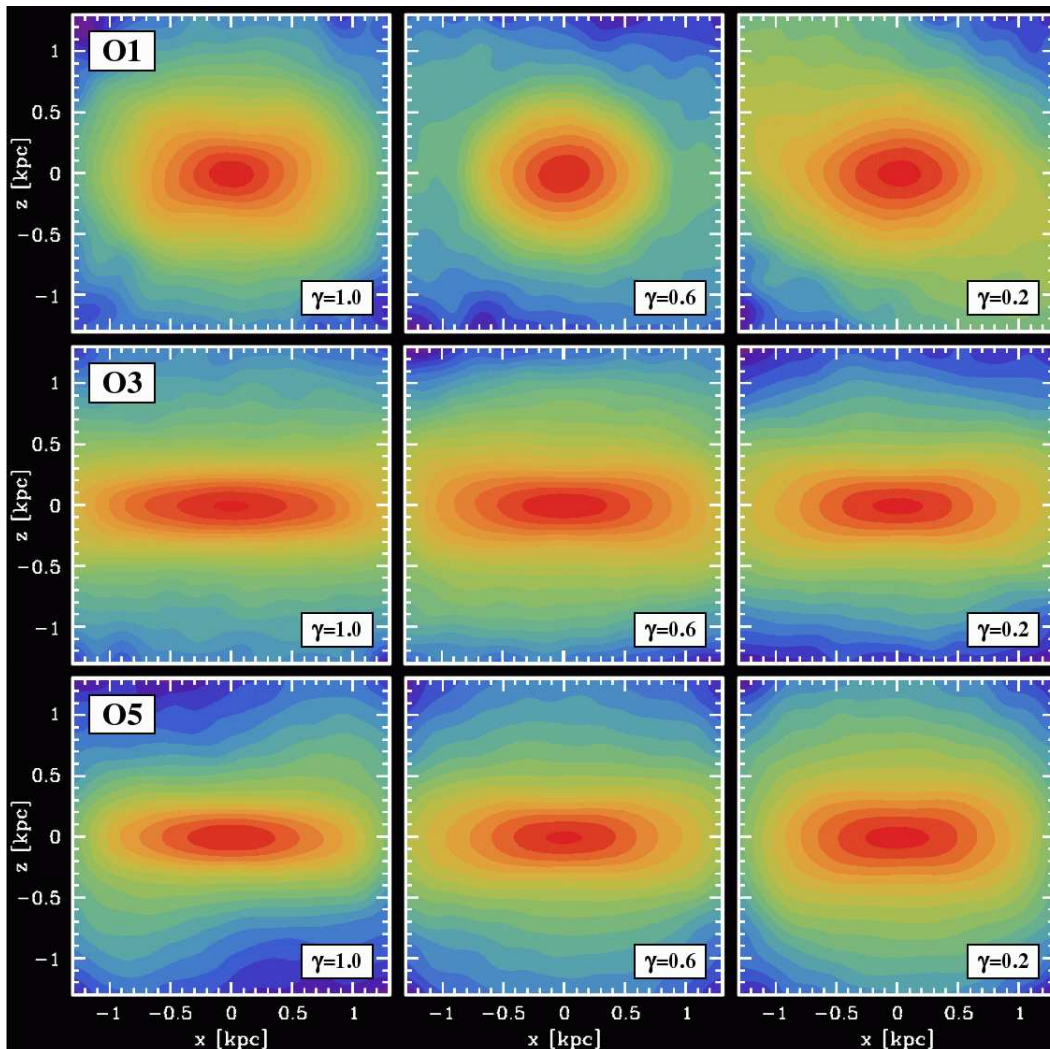


FIG. 3.— Surface number density distribution of stars in the simulated dwarfs. Results are presented for orbits O1 (upper panels), O3 (middle panels), and O5 (lower panels). All stellar components are depicted at $t = 10$ Gyr, except for that in the upper rightmost panel (O1; $\gamma = 0.2$) which is shown at $t = 6.35$ Gyr (corresponding to the timescale of the last apocenter before the disruption of the dwarf galaxy). The asymptotic inner slope of the dwarf DM density profile, γ , is indicated in each panel. The images show the most non-spherical views along the intermediate axis of the stellar distribution, y (where x and z denote the major and minor axes, respectively). The stars are binned into $0.2 \text{ kpc} \times 0.2 \text{ kpc}$ fields perpendicular to the line-of-sight. The contours correspond to the number of stars N within each bin and are equally spaced by 0.2 in $\log N$. The innermost contours are in the range $\log N = 3.6 - 4.6$ depending on the case.

lists the time elapsed from the beginning of the simulation until dSph formation occurs (the number of corresponding pericentric passages is included in parentheses). The entries in this column indicate, that similar to the likelihood, the efficiency of transformation into a dSph is considerably increased for disk dwarfs embedded in DM halos with shallow density profiles.

4. DISCUSSION

The present study is the first to elucidate the effect of the asymptotic inner slope γ of the dwarf DM density profile ($\rho \propto r^{-\gamma}$ as $r \rightarrow 0$) on the tidal evolution of dwarf galaxies consisting of baryonic components in the form of stellar disks. We have shown that, regardless of orbit inside the primary, rotationally-supported dwarfs embedded in DM halos with core-like density distributions ($\gamma = 0.2$) and mild density cusps ($\gamma = 0.6$) demonstrate a substantially enhanced likelihood and efficiency of transformation into dSphs relative to their counterparts with NFW-like steeper DM density profiles

($\gamma = 1$). Such shallow DM distributions are akin to those inferred from the mass modeling of observed LG dIrrs (e.g., Weldrake et al. 2003) and analogous galaxies outside of the LG (e.g., Oh et al. 2011). This fact highlights tidal stirring as a plausible mechanism for the origin of the morphology-density relation (e.g., Mateo 1998), an essential constraint that any model for the LG must satisfy.

The following order-of-magnitude calculations offer insight into our numerical results. In the impulse approximation, the energy injected at each pericentric passage is given by $\Delta E \propto M_{\text{host}}^2 M R^2 V_{\text{rel}}^{-2}$, where M_{host} is the mass of the host enclosed within r_{peri} , M denotes the mass of the dwarf within a characteristic radius R , and V_{rel} is the relative velocity of the two galaxies at the pericenter of the orbit (e.g., Binney & Tremaine 2008). For a specific set of initial orbital parameters, M_{host} and V_{rel} are fairly similar for different γ . Thus, $\Delta E \propto M R^2$. Moreover, by virtue of the virial theorem, the energy

content of the dwarf scales as $E \propto M^2/R$. Hence, the fractional increase in energy caused by the tidal shocks is $\Delta E/E \propto R^3/M$. At a given distance R from the center of our initial disk dwarf galaxies, decreasing cusp slopes correspond to smaller M , and thus to larger $\Delta E/E$. This explains why the $\gamma = 0.6$ and $\gamma = 0.2$ rotationally-supported dwarfs experience stronger tidal shocks and augmented mass loss relative to their $\gamma = 1$ counterparts, leading to their enhanced morphological transformation into dSphs. Considering adiabatic corrections to the energy change predicted by the impulse approximation (e.g., Gnedin & Ostriker 1999) would only reinforce this conclusion. Indeed, owing to the fact that such corrections are inversely proportional to a power of the stellar orbital frequency ω and ω is higher at a given radius for more concentrated mass distributions, decreasing cusp slopes would correspond to even larger $\Delta E/E$ compared to those predicted by the impulse approximation.

The results presented in this paper demonstrate that the orbital parameters and the DM density distributions of the progenitor rotationally-supported dwarfs can independently determine the final properties of dSphs formed via tidal stirring. Therefore, the fact that Fornax and Draco, for example, have roughly similar masses at present, as inferred from their stellar velocity dispersions (e.g., Kazantzidis et al. 2004b), but differ by about two orders of magnitude in luminosity, could be explained in two ways. One possibility is that the predecessors of these two dwarf galaxies acquired very different DM density profiles, for reasons related to their formation history and not to the environment. Alternatively, Fornax and Draco may have originated from systems that had comparable DM and baryonic mass distributions, but displayed dissimilar tidal evolutions and evolved differently because they entered their host galaxy on different orbits, perhaps due to a different infall epoch onto the primary. Other effects not included here, such as stripping due to ram pressure and external radiation fields at high redshift, may also affect the disk dwarf differently depending on their orbits (Mayer et al. 2006, 2007) and internal mass distributions, increasing further the scatter in the properties of the resulting dSphs.

The increased mass loss and rate of disruption experienced by dwarfs embedded in DM halos with shallow density profiles have important implications for alleviating the “missing satellites problem” (Moore et al. 1999; Klypin et al. 1999). These findings also suggest that the dwarf luminosity and mass functions must be shifted lower relative to those of Λ CDM simulations that do not take into account baryonic effects (such as outflows triggered by supernovae explosions; see Governato et al. 2010) which can give rise to flattening of DM cusps. Consequently, the recent claims regarding the agreement between theory and observations of the luminosity function and the radial distribution of satellites within MW-sized host halos (e.g., Macciò et al. 2010) may need revision.

Our investigation establishes tidal stirring as an even more prevalent transformation mechanism than previously considered. Indeed, earlier work adopting cuspy DM density profiles for the progenitor disk dwarfs has indicated that only orbits that are characterized by high eccentricities ($r_{\text{apo}}/r_{\text{peri}} \gtrsim 5$), typical of CDM structure formation models (e.g., Diemand et al. 2007), and small pericentric distances ($r_{\text{peri}} \lesssim 25$ kpc) are capable

of transforming rotationally-supported dwarfs into dSphs (e.g., Mayer et al. 2001; Kazantzidis et al. 2011a). For a transformation to occur, the same studies have also concluded that T_{orb} should be short enough to allow the disk dwarf galaxies to complete at least two pericentric passages inside their hosts. These two requirements are probably not met for a number of LG dSphs, a fact that questioned the widespread applicability of the tidal stirring model.

For example, the distant dSphs Leo I, Cetus, and Tucana (residing in the outskirts of the LG at several hundred kpc from the MW and M31; e.g., Caputo et al. 1999; McConnachie et al. 2005; Saviane et al. 1996) are likely moving on very wide orbits associated with extremely long T_{orb} . Moreover, proper-motion measurements have indicated a fairly large pericenter for Leo I ($r_{\text{peri}} \gtrsim 60$ kpc; Sohn et al. 2012) and a low-eccentricity orbit with a similarly great pericenter for the dSph Fornax (e.g., Piatek et al. 2007). Our results suggest that the origin of all these dSphs can be accommodated within the framework of the tidal stirring model (for alternative formation scenarios of the distant LG dSphs and Fornax, see, e.g., Kravtsov et al. 2004; Sales et al. 2007; Ludlow et al. 2009; Kazantzidis et al. 2011b and e.g., Yozin & Bekki 2012, respectively). Indeed, rotationally-supported dwarf galaxies on low-eccentricity and/or large-pericenter orbits may be efficiently transformed into dSph-type objects, provided that their DM halos possess shallow density profiles (see Table 2). In fact, assuming core-like DM distributions ($\gamma = 0.2$) and small r_{peri} , even a single pericentric passage can induce transformation into a dSph. We note that according to recent studies, Leo I has passed through the pericenter of its orbit once (Sohn et al. 2012) and the same conclusion may also apply to Cetus and Tucana (Teyssier et al. 2012).

The present work confirms the previously reported strong association between the development of bar instabilities in the disks of the progenitor late-type dwarfs and the formation of dSphs (e.g., Mayer et al. 2001; Klimentowski et al. 2009; Kazantzidis et al. 2011a). Bar-like structures should thus be common among the less evolved dwarf galaxies in the LG as the bar stage constitutes one of the longest phases in the transformation process. Recently, the first steps toward validating this fundamental prediction of tidal stirring have been taken with the detection of bars in a number of MW satellites, including Ursa Minor, Sagittarius, and Carina (Lokas et al. 2012b). Nonetheless, with the notable exception of the Large Magellanic Cloud, the number of irrefutable bar-like distortions observed in LG dwarfs is still relatively low (see, however, Klimentowski et al. 2009 for a discussion pertaining to the intrinsic difficulties in identifying bars in the dwarf galaxies of the LG).

Our simulations also indicate that none of the $\gamma = 1$ disk dwarfs are disrupted by the tidal field of the primary galaxy; of these, only systems on high-eccentricity ($r_{\text{apo}}/r_{\text{peri}} \gtrsim 5$) and small-pericenter ($r_{\text{peri}} \lesssim 25$ kpc) orbits are transformed into objects with the properties of dSphs. Interestingly, when $\gamma < 1$, the dSph-like systems that survive are generally on orbits with lower eccentricities and/or larger pericenters compared to those of typical CDM satellites (e.g., Diemand et al. 2007). This novel finding provides a natural explanation for the rather peculiar orbits of several classic LG dSphs such as

Fornax, Leo I, Tucana, and Cetus.

The degree of transformation into a dSph depends on both the number and the strength of tidal shocks, which are determined by T_{orb} and r_{peri} , respectively (e.g., Mayer et al. 2001; Kazantzidis et al. 2011a). Specifically, short orbital times and small pericentric distances, corresponding to orbits associated with a large number of strong tidal shocks, produce the strongest and most complete transformations. Assuming that the distant dSphs in the LG are products of tidal stirring and that their progenitors have no bias towards significantly shallower than average inner DM density distributions, we predict that these dwarfs should exhibit higher values of V_{rot}/σ_* relative to those of dSphs located closer to their hosts. Although tentative evidence of intrinsic rotation exists in Leo I (e.g., Koch et al. 2007), Cetus (Lewis et al. 2007), and Tucana (Fraternali et al. 2009), future conclusive measurements of kinematics in these dSphs will serve to validate (or falsify) this prediction.

Lastly, our approach neglects the effects of gas dynamics, star formation, and chemical evolution. Definitive

conclusions regarding the efficiency of the transformation process clearly require more sophisticated theoretical modeling, capable of capturing the turbulent, multi-phase structure of the interstellar medium in dwarf galaxies. Investigating the tidal stirring of realistic dIrr galaxies, such as those formed self-consistently in the cosmological hydrodynamical simulations of Governato et al. (2010), with recipes of radiative cooling, star formation, and supernovae feedback would thus be particularly valuable in this direction.

We acknowledge stimulating discussions with Giuseppina Battaglia, Jonathan Bird, Simone Callegari, Alan McConnachie, and Se-Heon Oh. S.K. is supported by the Center for Cosmology and Astro-Particle Physics at The Ohio State University. This work was partially supported by the Polish National Science Centre under grant NN203580940. The numerical simulations were performed on the “Glenn” cluster at the Ohio Supercomputer Center (<http://www.osc.edu>).

REFERENCES

- Binney, J. & Tremaine, S. 2008, *Galactic Dynamics: Second Edition* (Princeton University Press)
- Caputo, F., Cassisi, S., Castellani, M., Marconi, G., & Santolamazza, P. 1999, *AJ*, 117, 2199
- Colpi, M., Mayer, L., & Governato, F. 1999, *ApJ*, 525, 720
- Diemand, J., Kuhlen, M., & Madau, P. 2007, *ApJ*, 667, 859
- D’Onghia, E., Besla, G., Cox, T. J., & Hernquist, L. 2009, *Nature*, 460, 605
- Einasto, J., Saar, E., Kaasik, A., & Chernin, A. D. 1974, *Nature*, 252, 111
- Faber, S. M. & Lin, D. N. C. 1983, *ApJ*, 266, L17
- Fraternali, F., Tolstoy, E., Irwin, M. J., & Cole, A. A. 2009, *A&A*, 499, 121
- Gnedin, O. Y. & Ostriker, J. P. 1999, *ApJ*, 513, 626
- Governato, F. et al. 2010, *Nature*, 463, 203
- Ho, N. et al. 2012, *ApJ*, 758, 124
- Kazantzidis, S., Lokas, E. L., Callegari, S., Mayer, L., & Moustakas, L. A. 2011a, *ApJ*, 726, 98
- Kazantzidis, S., Lokas, E. L., Mayer, L., Knebe, A., & Klimontowski, J. 2011b, *ApJ*, 740, L24
- Kazantzidis, S., Magorrian, J., & Moore, B. 2004a, *ApJ*, 601, 37
- Kazantzidis, S., Mayer, L., Mastropietro, C., Diemand, J., Stadel, J., & Moore, B. 2004b, *ApJ*, 608, 663
- Klimontowski, J., Lokas, E. L., Kazantzidis, S., Mayer, L., & Mamon, G. A. 2009, *MNRAS*, 397, 2015
- Klimontowski, J., Lokas, E. L., Knebe, A., Gottlöber, S., Martinez-Vaquero, L. A., Yepes, G., & Hoffman, Y. 2010, *MNRAS*, 402, 1899
- Klypin, A., Kravtsov, A. V., Valenzuela, O., & Prada, F. 1999, *ApJ*, 522, 82
- Koch, A., Wilkinson, M. I., Kleyna, J. T., Gilmore, G. F., Grebel, E. K., Mackey, A. D., Evans, N. W., & Wyse, R. F. G. 2007, *ApJ*, 657, 241
- Kravtsov, A. 2010, *Advances in Astronomy*, vol. 2010, Article ID 281913 (astro-ph/0906.3295), 1
- Kravtsov, A. V., Gnedin, O. Y., & Klypin, A. A. 2004, *ApJ*, 609, 482
- Lewis, G. F., Ibata, R. A., Chapman, S. C., McConnachie, A., Irwin, M. J., Tolstoy, E., & Tanvir, N. R. 2007, *MNRAS*, 375, 1364
- Lokas, E. L. 2002, *MNRAS*, 333, 697
- Lokas, E. L., Kazantzidis, S., & Mayer, L. 2011, *ApJ*, 739, 46
- . 2012a, *ApJ*, 751, L15
- Lokas, E. L., Majewski, S. R., Kazantzidis, S., Mayer, L., Carlin, J. L., Nidever, D. L., & Moustakas, L. A. 2012b, *ApJ*, 751, 61
- Ludlow, A. D., Navarro, J. F., Springel, V., Jenkins, A., Frenk, C. S., & Helmi, A. 2009, *ApJ*, 692, 931
- Macciò, A. V., Kang, X., Fontanot, F., Somerville, R. S., Koposov, S., & Monaco, P. 2010, *MNRAS*, 402, 1995
- Mateo, M. L. 1998, *ARA&A*, 36, 435
- Mayer, L., Governato, F., Colpi, M., Moore, B., Quinn, T., Wadsley, J., Stadel, J., & Lake, G. 2001, *ApJ*, 559, 754
- Mayer, L., Kazantzidis, S., Mastropietro, C., & Wadsley, J. 2007, *Nature*, 445, 738
- Mayer, L., Mastropietro, C., Wadsley, J., Stadel, J., & Moore, B. 2006, *MNRAS*, 369, 1021
- Mayer, L., Moore, B., Quinn, T., Governato, F., & Stadel, J. 2002, *MNRAS*, 336, 119
- Mayer, L. & Wadsley, J. 2004, *MNRAS*, 347, 277
- McConnachie, A. W. 2012, *AJ*, 144, 4
- McConnachie, A. W., Irwin, M. J., Ferguson, A. M. N., & Ibata, R. A., Lewis, G. F., & Tanvir, N. 2005, *MNRAS*, 356, 979
- Mo, H. J., Mao, S., & White, S. D. M. 1998, *MNRAS*, 295, 319
- Moore, B., Ghigna, S., Governato, F., Lake, G., Quinn, T., Stadel, J., & Tozzi, P. 1999, *ApJ*, 524, L19
- Navarro, J. F., Frenk, C. S., & White, S. D. M. 1996, *ApJ*, 462, 563
- Oh, S.-H., de Blok, W. J. G., Brinks, E., Walter, F., & Kennicutt, Jr., R. C. 2011, *AJ*, 141, 193
- Orban, C., Gnedin, O. Y., Weisz, D. R., Skillman, E. D., Dolphin, A. E., & Holtzman, J. A. 2008, *ApJ*, 686, 1030
- Peñarrubia, J., Benson, A. J., Walker, M. G., Gilmore, G., McConnachie, A. W., & Mayer, L. 2010, *MNRAS*, 406, 1290
- Piatek, S., Pryor, C., Bristow, P., Olszewski, E. W., Harris, H. C., Mateo, M., Minniti, D., & Tinney, C. G. 2007, *AJ*, 133, 818
- Pontzen, A. & Governato, F. 2012, *MNRAS*, 421
- Read, J. I., Wilkinson, M. I., Evans, N. W., Gilmore, G., & Kleyna, J. T. 2006, *MNRAS*, 366, 429
- Sales, L. V., Navarro, J. F., Abadi, M. G., & Steinmetz, M. 2007, *MNRAS*, 379, 1475
- Saviane, I., Held, E. V., & Piotto, G. 1996, *A&A*, 315, 40
- Sohn, S. T., Besla, G., van der Marel, R. P., Boylan-Kolchin, M., Majewski, S. R., & Bullock, J. S. 2012, *ApJ* submitted (astro-ph/1210.6039)
- Stadel, J. G. 2001, Ph.D. Thesis, Univ. of Washington
- Teyssier, M., Johnston, K. V., & Kuhlen, M. 2012, *MNRAS*, 426, 1808
- Tolstoy, E., Hill, V., & Tosi, M. 2009, *ARA&A*, 47, 371
- Weldrake, D. T. F., de Blok, W. J. G., & Walter, F. 2003, *MNRAS*, 340, 12
- Widrow, L. M., Pym, B., & Dubinski, J. 2008, *ApJ*, 679, 1239
- Yozin, C. & Bekki, K. 2012, *ApJ*, 756, L18